Lock-in in forced vibration of a circular cylinder

Samvit Kumar, Navrose, and Sanjay Mittal

Citation: Phys. Fluids **28**, 113605 (2016); doi: 10.1063/1.4967729
View online: http://dx.doi.org/10.1063/1.4967729
View Table of Contents: http://aip.scitation.org/toc/phf/28/11
Published by the American Institute of Physics

PHYSICS OF FLUIDS **28**, 113605 (2016)

Lock-in in forced vibration of a circular cylinder

Samvit Kumar, Navrose, and Sanjay Mittal[a)]
Department of Aerospace Engineering, Indian Institute of Technology Kanpur, Uttar Pradesh 208016, India

(Received 3 June 2016; accepted 31 October 2016; published online 21 November 2016)

The phenomenon of lock-in/synchronization in uniform flow past an oscillating cylinder is investigated via a stabilized finite element method at $Re = 100$. Computations are carried out for various amplitudes and frequencies of cylinder oscillation to accurately obtain the boundary of the lock-in regime. Results from earlier studies show a significant scatter in the lock-in boundary. The scatter might be an outcome of the difference in data collection or the use of a different criterion for identifying lock-in. A new criterion for lock-in is proposed, wherein the following two conditions are to be satisfied. (i) The most dominant frequency in the power spectrum of lift coefficient matches the frequency of cylinder oscillation (f_y) and (ii) other peaks in the power spectrum, if any, are present only at super-harmonics of f_y. Utilizing this criterion, three flow regimes are identified on the frequency-amplitude plane: *lock-in, transition,* and *no lock-in*. The behaviour of the wake is also investigated by examining the power spectra of the velocity traces at various locations downstream of the cylinder. Wake-lock-in is observed during lock-in. A wake-transition regime is identified wherein the near wake, up to a certain streamwise location, is in a lock-in state while the downstream region is in a desynchronized state. For a fixed f_y, the location beyond which the wake is desynchronized moves downstream as the amplitude of oscillation is increased. The proposed criterion for lock-in addresses the wide scatter in the boundary of the lock-in regime among earlier studies. Energy transfer from the fluid to the structure, per cycle of cylinder oscillation, is computed from the data for forced vibration. The data is utilized to generate iso-energy transfer contours in the frequency-amplitude plane. The free vibration response with zero structural damping is found to be in very good agreement with the contour corresponding to zero energy transfer. *Published by AIP Publishing.* [http://dx.doi.org/10.1063/1.4967729]

I. INTRODUCTION

Flow past an oscillating cylinder is associated with several interesting phenomena. Amongst them, the one that has received considerable attention is *lock-in*. In addition to its relevance in the study of complex fluid-structure interaction problems, lock-in has several engineering applications as well.[1–3] During lock-in, the characteristics of the wake of the vibrating cylinder may be significantly different from that of a stationary cylinder. There have been a number of experimental and computational studies in the past to understand the phenomenon of lock-in. Some of these efforts attempt to identify the regime of lock-in. However, the criterion to identify lock-in state is not uniform in these studies. Therefore, there are discrepancies in the boundary demarcating the lock-in and no lock-in among various works. The main objective of the present work is to investigate a lock-in phenomenon via controlled vibrations of a circular cylinder and address the discrepancies in the lock-in boundary reported in earlier works.

Bishop and Hassan,[4] in their seminal experimental work, studied the fluid forces experienced by a cylinder undergoing a controlled vibration. Only transverse vibration was considered in the

a)Electronic mail: smittal@iitk.ac.in

study. They observed that for frequencies of cylinder oscillation (f_y) that are significantly different from the vortex shedding frequency associated with the flow past a stationary cylinder (f_{v_o}), the lift force fluctuates with a frequency nearly equal to f_{v_o}. On the other hand, for values of f_y close to f_{v_o}, the frequency of lift force synchronizes with the cylinder oscillation frequency. This phenomenon of the synchronization of frequencies has been referred to as *lock-in* or *wake-capture* or simply *synchronization* in the literature. Koopmann[5] examined the wake of an oscillating cylinder for various non-dimensional amplitudes, A^*, and frequencies, $f^*(= f_y/f_{v_o})$, using the smoke-flow visualization technique. The amplitude was non-dimensionalized by the diameter of the cylinder. It was observed that for each f^*, there exists a critical A^* below which the vortices in the wake are inclined to the axis of the cylinder. This mode of vortex shedding has been referred to as *oblique* vortex shedding in the literature.[6–8] Beyond the critical amplitude, the vortices are shed parallel to the cylinder axis. The oblique vortex shedding was identified as a no lock-in state while *parallel* vortex shedding was associated with the lock-in response. Figures 1(a) and 1(b) show the variation of critical A^* with f^* for $Re = 100$ and 200, respectively. It is noted that greater is the departure in the value of f^* from unity, larger is the amplitude required for lock-in.

Forced vibration has also been investigated via numerical simulations. Karniadakis and Triantafyllou[9] studied the velocity fluctuations at various streamwise locations in the wake of a vibrating cylinder for $Re = 100$. They proposed that during lock-in, the dominant frequency in the power spectrum of velocity fluctuations at all streamwise locations is f_y. Further, the spectrum shows peaks only at f_y and its super-harmonics. In the no lock-in state, the dominant frequency at all streamwise locations shifts to a value close to f_{v_o}. Between the lock-in and no lock-in states, the system goes through a transition regime where the dominant frequency can either be f_y or f_{v_o} depending on the streamwise location. In general, the dominant frequency in velocity fluctuation is f_y close to the cylinder and f_{v_o} and away from it. As the lock-in state is approached, the streamwise location where the dominant frequency is f_{v_o} shifts downstream. Figure 1(a) shows the boundary between the transition and the lock-in state for $Re = 100$ presented by Karniadakis and Triantafyllou.[9] Meneghini and Bearman[10] analyzed the lift force acting on a vibrating cylinder at $Re = 200$. Utilizing a criterion similar to Bishop and Hassan,[4] they presented the boundary between the lock-in and no lock-in states (Figure 1(b)). Nobari and Naderan[11] also used a criterion based on the lift force to differentiate between the lock-in and no lock-in states. According to their criterion, a peak at f_{v_o} in the power spectrum of the lift signal implies no lock-in while its absence implies lock-in. They analyzed the system for various values of A^* and f^*. Figure 1(a) shows the points in the A^*-f^* plane where Nobari and Naderan[11] observed a lock-in behavior.

Anagnostopoulos[12] compiled data from various studies and observed that there are discrepancies in the lock-in boundary reported by them. It was noted that numerical studies generally utilize frequency content in time variation of the lift coefficient to differentiate between the lock-in

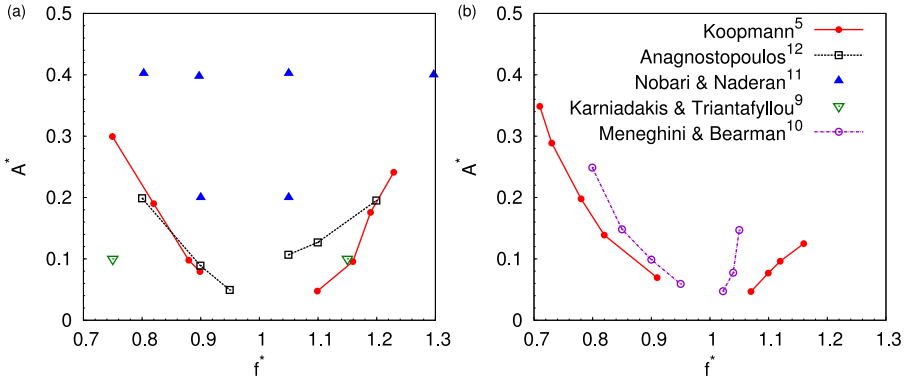

FIG. 1. Flow past a vibrating cylinder: boundary of lock-in regime reported in earlier studies for (a) $Re = 100$ and (b) $Re = 200$. The symbols used in the figure are •, Koopmann;[5] □, Anagnostopoulos;[12] ▲, Nobari and Naderan;[11] ▽, Karniadakis and Triantafyllou;[9] ○, Meneghini and Bearman.[10] The data points from the work of Nobari and Naderan[11] and Karniadakis and Triantafyllou[9] are for the lock-in state.

and no lock-in states. On the other hand, experiments usually rely on velocity fluctuations in the wake of the vibrating cylinder. Therefore, the difference in the lock-in boundary was attributed to the difference in the choice of the variables used to identify lock-in. To address this, Anagnostopoulos[12] utilized the frequency content of velocity fluctuations in the wake to analyze lock-in from a data set obtained from computations. The presence of a dominant peak at f_y was used to identify lock-in between the fluid and structure. The discrepancies in the lock-in boundary for $f^* < 1$ were resolved. However, the differences persisted for $f^* > 1$.

Table I summarizes the criterion used by various studies in the past to identify lock-in. The lock-in boundary from these studies is presented and compared in Figure 1. In general, different studies employ different criteria to identify lock-in. Further, the setup for data generation, computation, or experiment may also be different for many of these studies. This might be a cause of disagreement in the lock-in boundary reported by various studies. The present study investigates all these criteria for identifying lock-in using the same data set that is generated by direct time integration of the equations governing the dynamics of the coupled fluid-structure system. A new criterion of lock-in is proposed as well.

Controlled vibration study can be used to predict the response of a freely vibrating cylinder. In free vibration, the cylinder oscillates because of the unsteady fluid forces resulting from vortex shedding. Staubli[13] estimated the free vibration response using contour plots of the lift coefficient and the phase angle between the cylinder displacement and the lift coefficient obtained via forced vibration. The estimated response was found to be in very good agreement with the free vibration response reported by Feng.[14] Williamson and Roshko[15] investigated different types of vortex shedding modes in the wake of an oscillating cylinder. They presented boundaries demarcating the different modes on the A^*-f^* plane. Morse and Williamson[16,17] calculated the energy transfer between the fluid and the structure for the different modes of vortex shedding. They identified the modes of vortex shedding that are associated with positive transfer of energy from the fluid to the structure and therefore exist during free vibrations. The results were found to be in very good agreement with the free vibration experiments reported by earlier studies. A detailed description of the various modes of vortex shedding was presented by Williamson and Roshko[15] and Morse and Williamson.[16,17] Leontini *et al.*[18] studied the energy transfer between the fluid and the structure in the low Reynolds number regime ($100 \leqslant Re \leqslant 300$). They identified an additional mode of shedding that can also result in transfer of energy from the fluid to the cylinder. Prasanth and Mittal[19] compared the free vibration response for $50 \leqslant Re \leqslant 200$ with the lock-in boundary reported by Koopmann.[5] In general, good agreement was observed between the two results.

The objective of the present study is two fold. First, the phenomenon of lock-in is investigated in forced vibrations for $Re = 100$. Various criteria proposed in the literature for identifying lock-in boundaries for forced oscillations are compared on the A^*-f^* plane for the same data set. Energy transfer from the fluid to the oscillator, per cycle of cylinder oscillation, is computed for forced oscillations. The contours of iso-energy transfer are presented on the A^*-f^* plane. The second objective of the study is to compare the forced and free vibrations. The response computed for free

TABLE I. Different criteria for lock-in that have been employed in earlier studies.

Study	Experimental or numerical	Criterion for lock-in
Bishop and Hassan[4]	Experimental	Frequency of lift fluctuation matches the cylinder oscillation frequency (f_y)
Koopmann[5]	Experimental	Vortex shedding changes from oblique to parallel shedding
Karniadakis and Triantafyllou[9]	Numerical	Dominant frequency of the velocity fluctuations at various locations match f_y
Meneghini and Bearman[10]	Numerical	Frequency of lift fluctuation matches f_y
Anagnostopoulos[12]	Numerical	Dominant frequency of the velocity trace at a point in the wake matches f_y
Nobari and Naderan[11]	Numerical	Lock-in is identified by the absence of a peak at f_{v_o} (vortex shedding frequency for a stationary cylinder in the power spectrum of lift fluctuations)

vibrations, at the same Re, is plotted on the A^*-f^* plane along with the iso-energy transfer contours and the lock-in boundaries from the forced vibration study.

II. NUMERICAL SETUP

A. Governing equation and solution strategy

The flow is modeled using the incompressible Navier-Stokes equations in primitive variables form. Only transverse vibration of the cylinder has been considered. In the controlled vibration study, the cylinder oscillates sinusoidally with a prescribed normalized amplitude (A^*) and frequency (F_y). The normalized displacement of the cylinder as a function of the time is given as

$$Y = A^* \sin(2\pi F_y t). \tag{1}$$

F_y is defined as $f_y D/U$, where f_y is the frequency of cylinder oscillation, D the diameter of the cylinder, and U the free-stream speed. The cylinder displacement is normalized with D. A schematic of the setup, for forced vibration, is shown in Figure 2.

For numerical simulation of free vibration, the cylinder is mounted on an elastic support that is modeled via a linear spring and damper. The equation governing the motion of the cylinder is

$$\ddot{Y} + 4\pi F_N \zeta \dot{Y} + (2\pi F_N)^2 Y = \frac{2C_L}{\pi m^*}. \tag{2}$$

Here, F_N is the reduced natural frequency of the oscillator, ζ the structural damping ratio, and C_L the instantaneous lift coefficient. C_L is computed by integrating stresses around the circumference of the cylinder. $\ddot{Y}$ and $\dot{Y}$ denote the normalized transverse acceleration and velocity, respectively. F_N is defined as $f_n D/U$, where f_n is the natural frequency of the oscillator in vacuum. The mass ratio m^* is the ratio of the mass of the cylinder to the mass of the fluid displaced by it. To encourage a large amplitude oscillation in free vibration, the structural damping ratio is assigned a zero value.

A stabilized space-time finite element method has been used to carry out the computations (Tezduyar *et al.*[20,21]). The detailed description of the governing equations and finite element formulation used in the present study can be found in the work of Prasanth and Mittal.[19] The numerical stabilizations are based on the SUPG (Streamline–Upwind/Petrov–Galerkin) and PSPG (Pressure–Stabilizing/Petrov–Galerkin) techniques (Tezduyar *et al.*[22]). The equation of motion for the oscillator, given by Equation (2), is also cast in the space-time formulation as described in the work of Mittal[23] and Mittal and Tezduyar.[24]

B. Computational domain and finite element mesh

A sketch of the computational domain is shown in Figure 2. The cylinder is placed in a rectangular computational domain whose upstream and downstream boundaries are located at a distance of $20D$ and $70D$ from the center of the cylinder, respectively. The lateral width of the domain is $20D$. The computational domain is the same as that used by Prasanth and Mittal[19] for free vibration simulations in the laminar flow regime ($60 \leq Re \leq 150$). The domain is discretized using a finite element mesh that consists of 11 256 nodes and 10 988 quadrilateral elements. The mesh has a finer

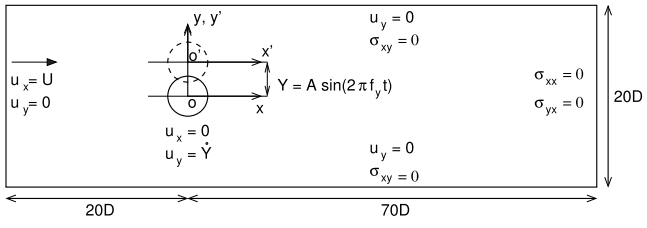

FIG. 2. Schematic of the setup for forced vibration of the cylinder. The sketch is not to scale. u_x and u_y are the components of flow velocity in the x and y directions, respectively. σ is the stress tensor.

spatial resolution compared to the mesh used by Prasanth and Mittal.[19] The details of the mesh and the effect of spatial and temporal resolution on the results are presented in the Appendix. To account for the deformation of the domain owing to the movement of the cylinder, a mesh moving scheme is used. In this method, the mesh close to the cylinder moves along with it like a rigid body while the outer boundary remains fixed. This scheme has been successfully used in our earlier studies (Prasanth and Mittal,[19] Navrose and Mittal,[25] Furquan *et al.*[26]). It is expected to give almost no projection errors in the solution in the vicinity of the cylinder (Tezduyar *et al.*[20,21]).

C. Boundary conditions

Figure 2 shows the schematic of the computational setup along with the boundary conditions. At the upstream boundary, free-stream values are assigned to the velocity. No-slip condition is applied on the velocity at the surface of the cylinder. In free vibrations, the displacement and velocity of the cylinder are updated in each non-linear iteration of the time marching process. The stress vector is set to zero at the downstream boundary. On the lateral boundaries, the component of velocity normal to the boundaries and the component of the stress along the boundaries are prescribed a zero value.

III. A NEW CRITERION FOR LOCK-IN

Table I lists the various criteria for lock-in that have been utilized in earlier studies. As noted in Section I, the lock-in boundaries obtained via different criteria do not agree. To address the discrepancies, we propose an alternate criterion to identify lock-in. The system is said to be in a state of lock-in when the following two conditions are satisfied: (a) the dominant frequency in the power spectrum of lift coefficient matches the cylinder oscillation frequency f_y and (b) other peaks in the power spectrum, if any, are present only at integral multiples of f_y. The regime where only the first of the two conditions is satisfied is referred to as *transition* regime. All other situations correspond to a no lock-in state.

IV. RESULTS

A. Lock-in boundary with the proposed criterion

Computations are carried out for flow past a vibrating cylinder for various f^* and A^*. The Reynolds number for all simulations is $Re = 100$. For each (f^*, A^*), power spectrum of the lift coefficient is examined once the flow has achieved a fully developed state. Lock-in is then identified based on the criterion proposed in Section III. Figure 3 shows the boundary of the lock-in regime along with flow and the power spectrum of C_L at a few selected values of (f^*, A^*). For a fixed f^*, lock-in occurs if A^* exceeds a certain threshold value. The threshold A^* required for lock-in increases with increased departure of f^* from unity. The lock-in boundary is similar to that presented by Koopmann[5] and Meneghini and Bearman.[10]

The transition from no lock-in to lock-in state is qualitatively different (Figure 3) on the two sides of $f^* = 1$. For $f^* < 1$, the transition is fairly sharp. For example, at $f^* = 0.8$ the flow is in a state of no lock-in for $A^* = 0.15$. The power spectrum of C_L for $(f^*, A^*) = (0.8, 0.15)$ has the largest peak at f_{v_o}. Other peaks in the spectrum are present at f_y and several other frequencies that are not necessarily super-harmonics of f_y (Figure 3(a)). A slight increase in A^* to 0.20, while keeping f^* fixed at 0.8, results in a lock-in state. The most dominant frequency in the power spectrum of C_L shifts to f_y (Figure 3(b)). Further, other peaks in the spectrum are present at integral multiples of f_y only. Figure 3 shows the vorticity field at the time instant when the cylinder is at its mean position and moving in the positive y direction. The mode of vortex shedding in both no lock-in and lock-in states is $2S$, wherein two vortices of opposite circulation are shed per cycle of cylinder oscillation. However, the spatial regularity in the arrangement of vortices is different in the lock-in and no lock-in state. The vortices are spaced regularly during lock-in $\left((f^*, A^*) = (0.8, 0.15)\right)$. On

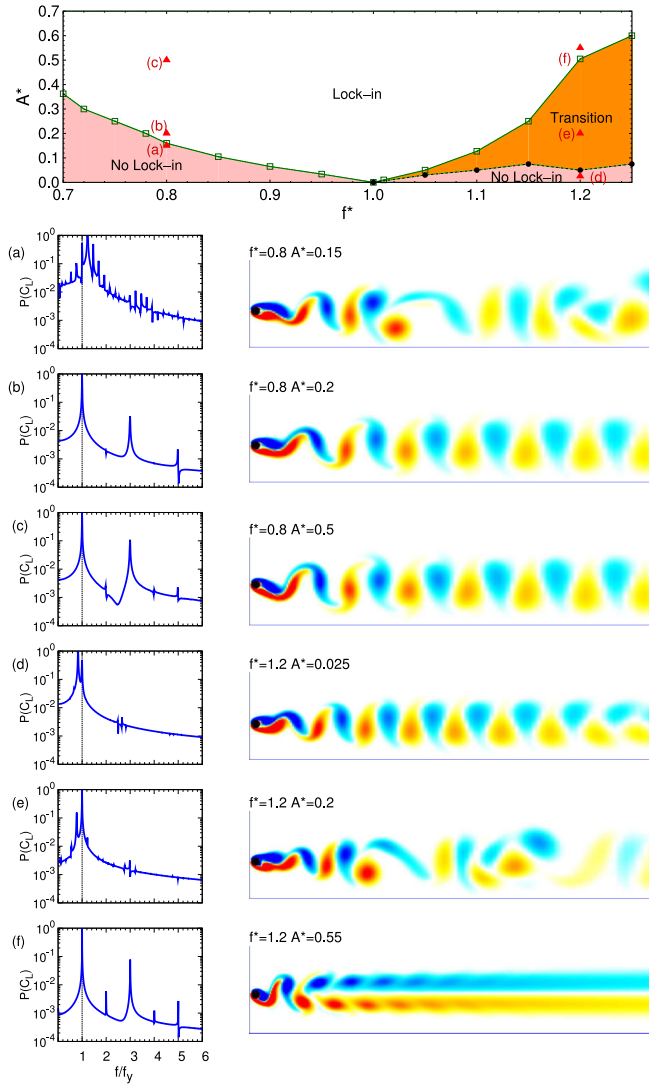

FIG. 3. Re = 100 flow past a vibrating cylinder: top row shows the lock-in, transition, and no lock-in regimes in the (f^*, A^*) plane. The power spectra of C_L and the instantaneous vorticity field for certain values of (f^*, A^*) are shown in (a) $(f^*, A^*) = (0.8, 0.15)$, (b) $(f^*, A^*) = (0.8, 0.2)$, (c) $(f^*, A^*) = (0.8, 0.5)$, (d) $(f^*, A^*) = (1.2, 0.025)$, (e) $(f^*, A^*) = (1.2, 0.2)$, and (f) $(f^*, A^*) = (1.2, 0.55)$.

the other hand, the arrangement is irregular for $(f^*, A^*) = (0.8, 0.20)$ when the flow is in a state of no lock-in. This becomes more apparent from Figures 4(a) and 4(b) that show the time histories of force coefficients for $A^* = 0.15$ and 0.20, respectively. The time variation of C_L is regular in the lock-in state. However, for $A^* = 0.15$ time histories of force coefficients show amplitude and frequency modulation. Within the lock-in regime, the strength of vortices and the lateral width of the wake increase with an increase in A^* (Figure 3(c)).

The situation is very interesting for $f^* > 1$. For a given value of f^*, the transition from no lock-in to lock-in takes place over a range of A^*. Below $A^* = A^*_{transition}$, even though the power spectrum of $C_L(t)$ shows a peak at f_y, the dominant frequency is close to f_{v_o}. The system, therefore, is in a state of no lock-in. At $A^*_{transition}$, the signal strength at f_{v_o} and f_y is identical. The variation of $A^*_{transition}$ with f^* is also marked in Figure 3. For $A^* > A^*_{transition}$, the dominant frequency in power spectrum of $C_L(t)$ is close to f_y. This meets the first criterion of lock-in as proposed in Section III. However, the power spectrum has peaks at frequencies that are not super-harmonic of f_y, thereby not satisfying the second criterion for lock-in. This regime is referred to as *transition* regime. Within

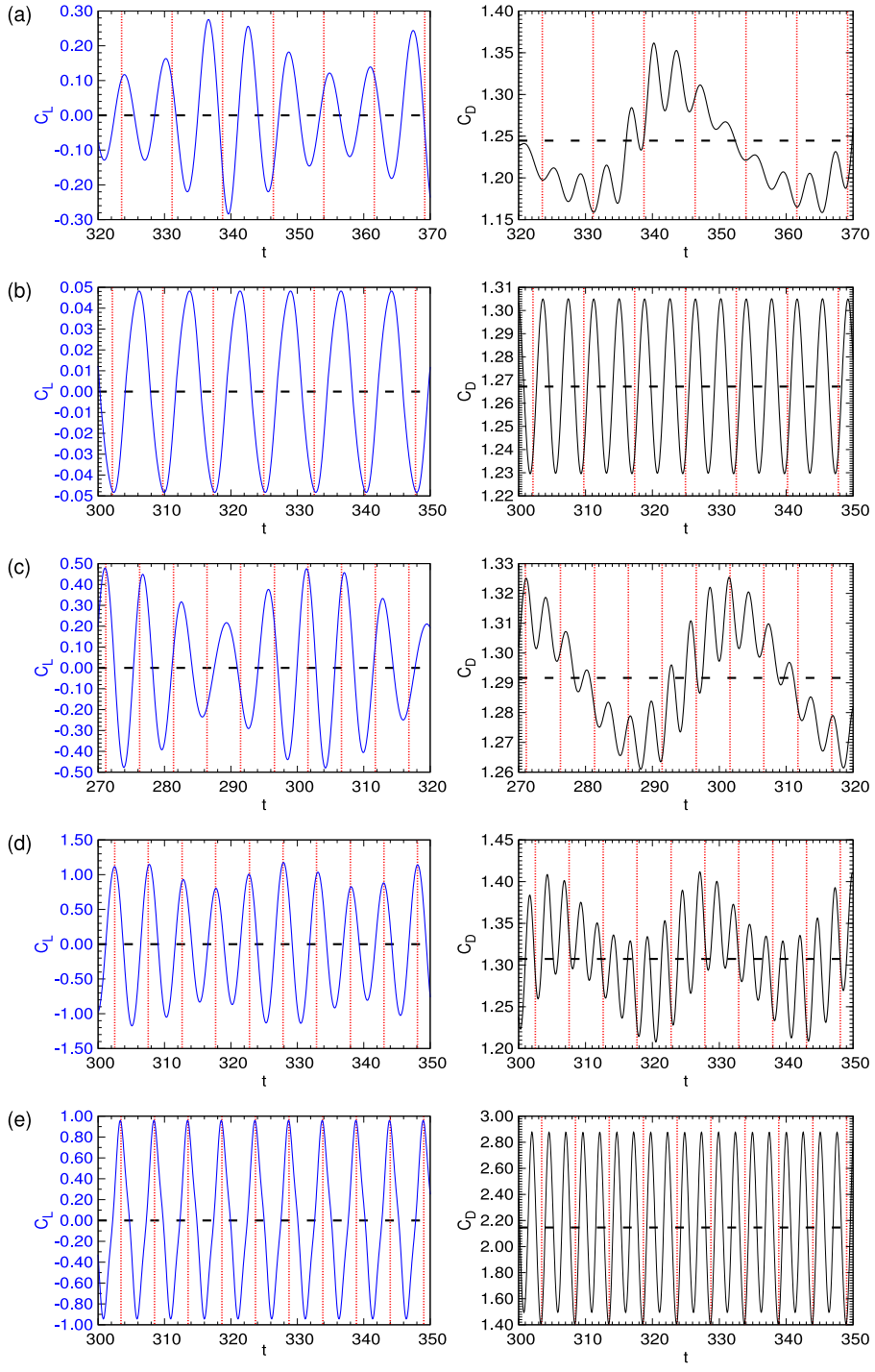

FIG. 4. Re = 100 flow past a vibrating cylinder: time variation of lift and drag coefficient for certain values of (f^*, A^*). $(f^*, A^*) =$ (a) $(0.8, 0.15)$ in the state of no lock-in, (b) $(0.8, 0.2)$ in lock-in, (c) $(1.2, 0.025)$ in the state of no lock-in, (d) $(1.2, 0.2)$ in the transition regime, and (e) $(1.2, 0.55)$ in lock-in. The vertical broken lines represent time instants at which the cylinder is at its maximum positive excursion while the horizontal broken lines show the time-average of the respective quantities.

the transition regime, the power contained in frequency f_{v_o} decreases with an increase in A^* and it vanishes completely at the boundary of the lock-in regime. Figures 3(d)–3(f) show the power spectrum of C_L and the vorticity field for $f^* = 1.2$ and $A^* = 0.025$, 0.2, and 0.55, respectively. The

flow is in *no lock-in*, *transition*, and *lock-in* state, respectively, for these values of A^*. The $2S$ mode of vortex shedding is observed in the no lock-in and transition regimes. The time-histories of force coefficients are shown in Figures 4(c) and 4(d) for $A^* = 0.025$ and 0.2, respectively. Both signals exhibit low frequency modulation. The shedding is irregular for both cases. During lock-in, the mode of shedding is $C(2S)$ and the time histories of the force coefficients show a periodic behavior (Figure 4(e)).

B. Frequency response of velocity in the wake

A few studies in the past have utilized the time trace of velocity in the wake of a vibrating cylinder to identify lock-in (for example, the work of Karniadakis and Triantafyllou[9] and Anagnostopoulos[12]). We analyze the power spectrum of the cross-stream component of velocity at several locations in the wake for different (f^*, A^*). The transverse location of all the probes is $0.63D$ with respect to the center of the cylinder. It is found that although there are some similarities, there are also certain significant differences between the spectra of C_L and velocity in the wake. To avoid any possible confusion with lock-in defined on the basis of time histories of C_L, we introduce the terms *wake-lock-in, wake-no-lock-in*, and *wake-transition*. These are based on the spectra of the velocity traces in the wake. Fig. 5 shows the wake lock-in boundary along with the power spectra of the velocity, for certain values of (f^*, A^*). The various flow regimes are described below.

Wake-lock-in regime: This regime coincides with the lock-in regime determined by C_L. The dominant frequency at all locations in the wake is f_y. In addition, as is seen for C_L, the peaks in the frequency spectra occur only at superharmonics of f_y at all probe locations. Figures 5(d) and 5(h) show the power spectra at various probe locations in the wake for $f^* = 0.8$ and 1.2, respectively. The lock-in and wake-lock-in boundaries are found to be identical.

Wake-no-lock-in regime: The dominant frequency in the wake at most streamwise locations downstream of the cylinder is f_{v_o}. In addition, the power spectra show peaks at other frequencies that are not necessarily superharmonics of f_y. Figures 5(a) and 5(e) show the power spectra at various probe locations for $f^* = 0.8$ and 1.2, respectively.

Wake-transition regime: The dominant frequency in the power spectrum depends strongly on the streamwise location of the probe. For a given (f^*, A^*), the dominant frequency in the time trace of the velocity is f_y only up to a certain streamwise distance from the cylinder. Probes located beyond this streamwise location show a velocity variation whose dominant frequency is mostly f_{v_o}. In all cases, the power spectra show additional peaks that are not necessarily superharmonics of f_y. Figures 5(b) and 5(c) show this phenomenon for $f^* = 0.8$. The same is shown for $f^* = 1.2$ in Figures 5(f) and 5(g). In the wake-transition regime, the wake is synchronised with the oscillation of the cylinder up to a certain streamwise location, while it is not synchronised beyond that. With increase in A^*, while keeping f^* fixed, the streamwise extent of this region of synchronization increases.

An interesting question arises regarding the wake-transition regime: "*Does the streamwise extent of the region of synchronization increase gradually with increase in A^*?*" To address this we study, at $f^* = 0.8$ and 1.2, the streamwise location of probes where the dominant frequency of time variation of transverse velocity is f_y, i.e., they are synchronized with cylinder oscillation. The data from the study are shown in Figure 6. The background grid on the x/D-A^* plane shows streamwise location of the probes that have been monitored for various A^*. The points where the probe data are associated with a dominant frequency of f_y are marked in solid squares. It is seen that with increase in A^*, the wake region that exhibits synchronization extends further downstream. However, it does so in jumps and not gradually. For example, at $f^* = 1.2$, the wake for $A^* = 0.4$ (Figure 6(b)) is synchronized with cylinder vibration up to a distance of $3.84D$ from the center of the cylinder. However, the extent of synchronization jumps to $7.68D$ for $A^* = 0.45$ and remains the same for $A^* = 0.5$. We note that in the A^*-f^* plane, unlike the classification based on C_L, the velocity traces show a wake-transition regime for $f^* < 1$ as well. The wake transition boundaries for $f^* > 1$ are identical to the boundaries of the transition regime.

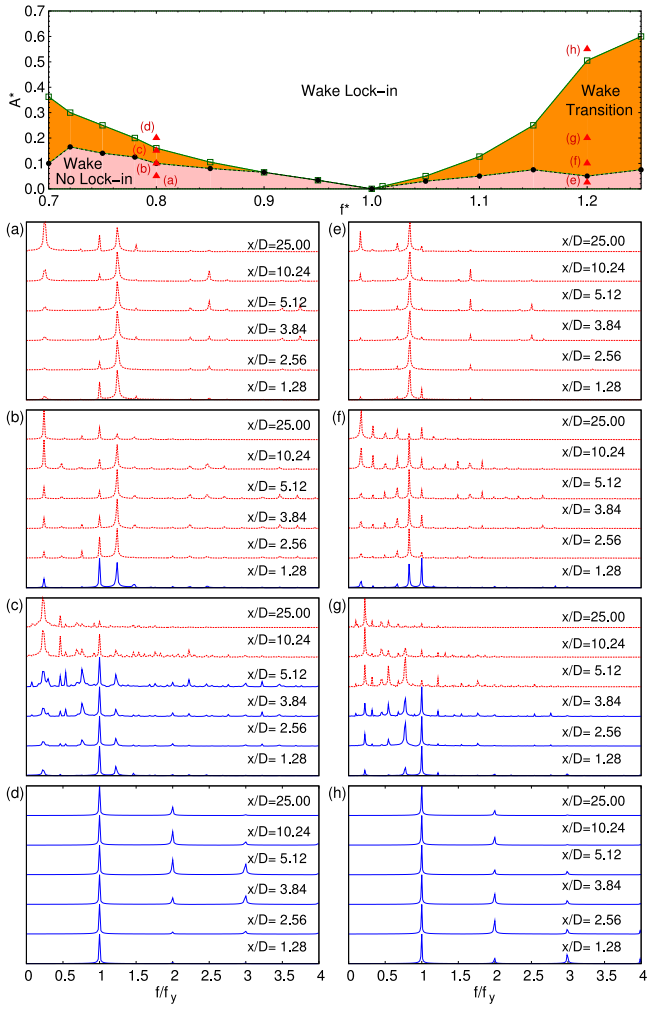

FIG. 5. Re = 100 flow past a vibrating cylinder: top row shows the wake-lock-in, wake-no-lock-in, and wake-transition regimes on the (f^*, A^*) plane. The power spectra of the cross-stream component of velocity at various streamwise locations in the wake are shown for $(f^*, A^*) =$ (a) $(0.8, 0.05)$, (b) $(0.8, 0.1)$, (c) $(0.8, 0.15)$, (d) $(0.8, 0.2)$, (e) $(1.2, 0.05)$, (f) $(1.2, 0.1)$, (g) $(1.2, 0.2)$, and (h) $(1.2, 0.55)$.

C. Comparison of various criteria for identifying lock-in

Figure 1 shows that there is a significant scatter in the boundaries demarcating the regions of no lock-in and lock-in. The scatter may be attributed to a difference in the experimental/computational methods and the related setup for generating the flow data, and/or the different criteria for identifying the lock-in boundaries. We suspect that the primary source of disagreement between the various studies might be the different criteria for lock-in that have been used. To address this, we apply the various criteria listed in Table I to data obtained from the present simulations. The outcome is summarized in Figure 7. The lock-in boundary predicted by the various criteria are in reasonable agreement for $f^* < 1$. However, significant differences are observed between some of the predictions for $f^* > 1$. There is an excellent agreement in the lock-in boundary predicted via the criteria used by Karniadakis and Triantafyllou,[9] Nobari and Naderan,[11] and the present study. The criterion used by Meneghini *et al.*[10] predicts this boundary to be the one between the no lock-in and transition regimes. The method of Anagnostopoulos[12] that relies on velocity trace at one location in the wake results in a similar prediction. As discussed earlier in Section IV B, the entire wake does not lock-in to f_y in the wake-transition regime; the streamwise extent of the wake region that synchronizes depends on A^*. Therefore, the criterion proposed by Karniadakis and Triantafyllou,[9] based on time

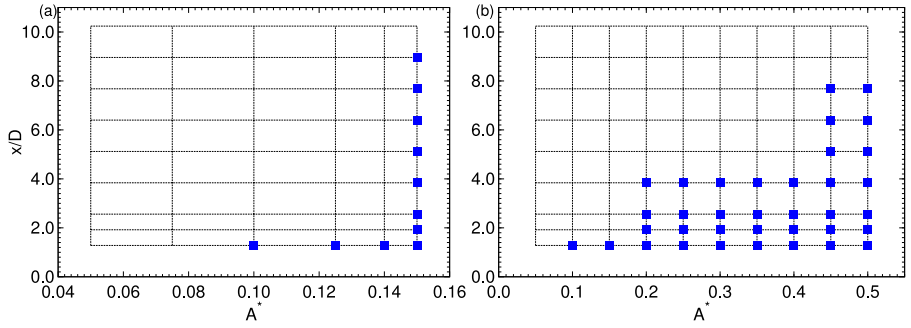

FIG. 6. Re = 100 flow past a vibrating cylinder with (a) $f^* = 0.8$ and (b) $f^* = 1.2$: cross-stream component of velocity is sampled at various streamwise locations for different A^*. The crossing of the grid lines denote the cases that have been studied. The solid squares denote the streamwise locations where the dominant frequency of the time trace of the cross-stream component of velocity equals f_y.

traces of velocity at various locations in the wake, and that from the work of Anagnostopoulos[12] which uses only one location in the wake, lead to different predictions. C_L is an integrated quantity and seems to carry the information regarding the frequency content for the entire wake. Thus, it appears to be a good candidate for identification of lock-in.

D. Energy transfer

1. Forced vibration

An important quantity associated with free vibrations is the energy transfer between the structure and surrounding flow. It is possible to estimate the free vibration response from the data for forced vibration by matching the energy transfer per cycle of cylinder oscillation (E_c). E_c is defined as

$$E_c = \int_0^{T_c} C_L(t)\dot{Y}(t)dt. \tag{3}$$

Here, T_c is the time period of cylinder oscillation. A positive value of E_c implies net transfer of energy from the flow to the cylinder while a negative value signifies net energy transfer from the cylinder to the flow.

Figure 8 shows the energy map for a vibrating cylinder on the A^*-f^* plane. It is generated by computing E_c for various (f^*, A^*) and interpolating them using the least squares method. The lock-in boundary is shown in the figure using solid thick lines. Also shown is the boundary that demarcates the no lock-in and transition regime. It is observed that both positive and negative values of E_c are possible in the lock-in regime. In general, within the lock-in regime, lower amplitude of cylinder oscillation is associated with positive E_c while higher values of A^* result in negative E_c.

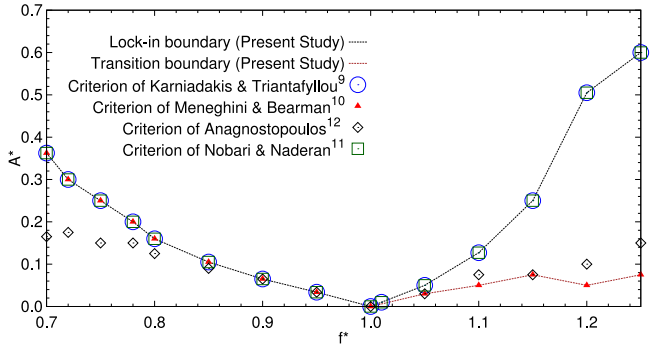

FIG. 7. Re = 100 flow past a vibrating cylinder: lock-in boundaries obtained using different criteria listed in Table I on the present data set.

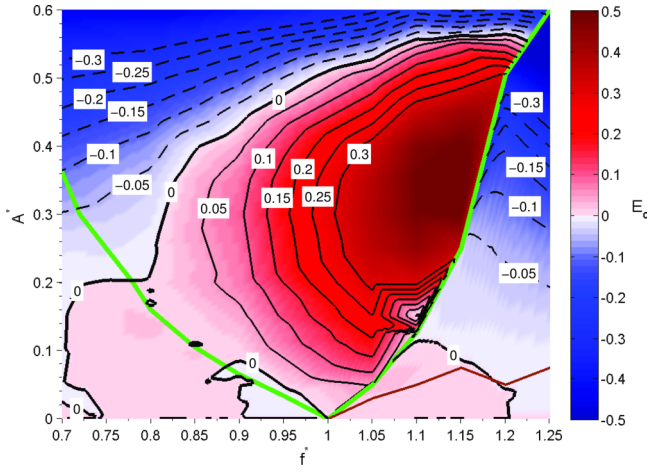

FIG. 8. Re = 100 flow past a vibrating cylinder: map of energy transfer per cycle of cylinder oscillation on the $f^* - A^*$ plane. Iso-energy contours with positive values are shown as solid lines while negative energy contours are shown using broken lines. The contour of zero energy transfer is marked with a thick black line. The green line shows the lock-in boundary and the brown line marks the boundary between no lock-in and transition.

Of great interest is the contour corresponding to zero net energy transfer ($E_c = 0$). This is shown using a thick solid line. Later in the paper we use the contour to compare free vibration response of a cylinder with forced vibrations associated with $E_c = 0$. A striking feature of Figure 8 is its asymmetry with respect to $f^* = 1.0$. While E_c shows a gradual change across the lock-in boundary for $f^* < 1.0$, the change is rather abrupt for $f^* > 1.0$.

2. Free vibration

Morse and Williamson[17] used the energy contours obtained via controlled vibration of a cylinder to estimate the response of a freely vibrating cylinder. The analysis was carried out at relatively large Reynolds number ($Re \sim 4000$) and for a finite value of structural damping ratio. The estimated response was found to be in very good agreement with free vibration response reported by Govardhan and Williamson.[27] In this work, we compare the data for free and forced vibration in the laminar flow regime. The response of a freely vibrating cylinder for $Re = 100$ is obtained by carrying out direct time integration of the equations governing the dynamics of flow and the cylinder (Equation (2)). The mass ratio is set to $m^* = 10.0$ and the structural damping is assumed to be zero. Figure 9(a) shows the variation of the amplitude of cylinder oscillation with reduced velocity. The reduced velocity is defined as $U^* = U/f_n D$. It is the inverse of the reduced natural frequency of the oscillator. The different branches of cylinder response and the desynchronization regimes are marked in the figure. A detailed description of the various branches has been presented in our earlier work (Prasanth and Mittal;[19] Navrose *et al.*[28]). Recently, we have identified a new branch, *initial branch (II)*, in free vibration response of a cylinder (Navrose and Mittal[29]). The new branch has also been included in Figure 9(a). The response is very similar to that observed by Singh and Mittal.[30]

Figure 9(b) shows the data points of free vibration on the energy map, in the $f^* - A^*$ plane, obtained via forced oscillations. Typically, the limit cycle response of a freely vibrating cylinder is nearly sinusoidal. We recall that in controlled oscillation study, the cylinder is allowed to oscillate sinusoidally as well. Therefore, the flow does not see the difference between a freely vibrating cylinder and controlled oscillation of the cylinder if the amplitude and frequency for the two is same. Consequently, the time variation of force coefficients and the energy transfer between the fluid and the cylinder per cycle of cylinder oscillation are the same in the two cases. Since the structural damping coefficient is assumed to be zero in the present computation for free vibration, the limit cycle response is associated with $E_c = 0$. The free vibration response, therefore, is expected to lie along $E_c = 0$ contour on the energy map. This, as observed in Figure 9(b), is

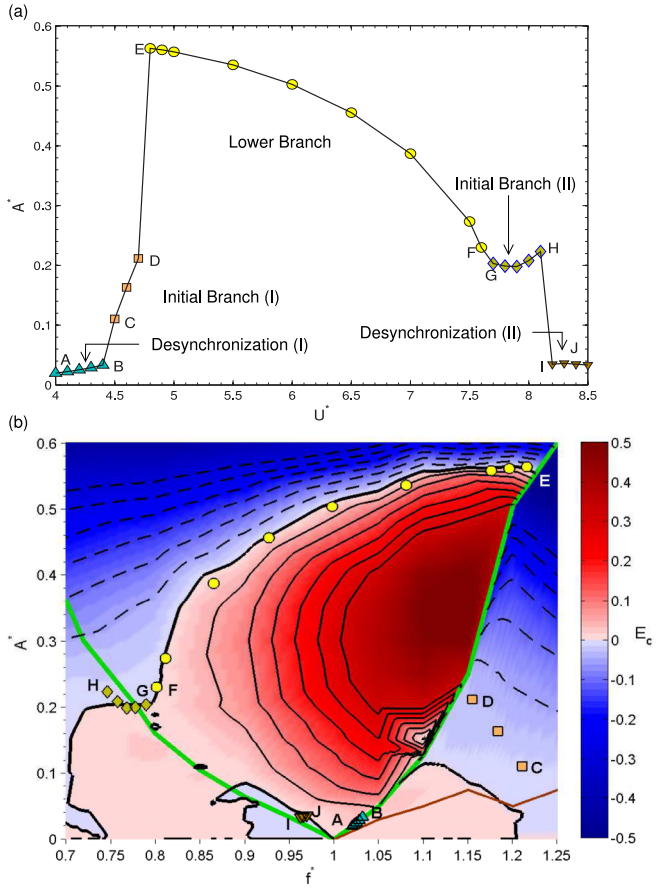

FIG. 9. $Re = 100$ flow past a cylinder undergoing (a) free vibration and (b) forced vibration. In (a), the variation of maximum amplitude of cylinder oscillation with reduced velocity is shown. In (b), energy map consisting of data points from free vibration study.

indeed the case for desynchronization regimes, lower branch, and initial branch (II). On initial branch (I), the time histories of cylinder displacement and force coefficients show modulation. The assumption of sinusoidal cylinder displacement does not hold too well for $IB(I)$. Therefore, the points corresponding to $IB(I)$ appear in regions where E_c is close to but not exactly zero.

V. CONCLUSION

Lock-in phenomenon is investigated via controlled vibration of a circular cylinder placed in uniform flow at $Re = 100$. Compilation of results from earlier studies show discrepancies in the boundary of the lock-in regime reported by them. A new criterion for lock-in is proposed. According to this proposal, lock-in occurs when (i) the dominant frequency in the power spectrum of lift coefficient matches the cylinder oscillation frequency f_y and (ii) the other peaks in the power spectrum, if any, are present only at integral multiples of f_y. It is observed that for $f_y/f_{v_o} < 1$, f_{v_o} being the vortex shedding frequency associated with flow past a stationary cylinder, the transition from no lock-in to lock-in state occurs abruptly. The mode of vortex shedding switches from irregular $2S$ mode to a regular $2S$ mode across the lock-in boundary. For $f_y/f_{v_o} > 1$, with increase in the amplitude of cylinder oscillation (A^*), the response first moves from no lock-in to a transition regime. In the transition regime, the power spectrum of C_L shows a dominant frequency at f_y. However, it also shows other peaks at frequencies that are not necessarily super-harmonics of f_y. The strength of the component of signal corresponding to a frequency of f_{v_o} decreases with an increase

in A^* in the transition regime and becomes zero at the lock-in boundary. The system remains in the lock-in state for higher values of A^*. By employing the criteria for lock-in from earlier studies on the present data set, it is observed that some of these studies have reported the boundary between the no lock-in and transition regime as the lock-in boundary. The proposed criterion clearly defines the no lock-in, transition, and lock-in states and thus differentiates between the two boundaries. It would be interesting to employ this criterion for identifying response regimes at higher values of Re where the flow is expected to be three-dimensional. Large amplitude oscillation of the cylinder is expected to contribute to spanwise coherence of the flow. Therefore, the criterion based on C_L should work well to differentiate between the lock-in and no lock-in regimes. It remains to be seen how the transition regime pans out at high Re.

The wake of a vibrating cylinder is analyzed by examining the power spectrum of the cross-stream component of velocity at several streamwise locations. The wake synchronizes with the cylinder vibration at all streamwise locations when the flow is in a lock-in state. We also refer to this as wake-lock-in. The power spectrum of cross-stream velocity shows peaks at f_y as well as its super-harmonics. The flow is in a state of no lock-in for low amplitude vibration of the cylinder. In this state the wake is desynchronized with cylinder oscillations at all streamwise locations. We refer to this state, of the wake as wake-no-lock-in. The wake-transition regime is observed for intermediate values of cylinder oscillation amplitude. In this regime, the near wake is synchronized while the downstream region of the wake is in a desynchronized state. With increase in A^*, while keeping f_y/f_{v_o} fixed, the streamwise location in the wake, where the response switches from synchronization to desynchronization, shifts downstream. The shift, however, is not gradual and occurs in steps with change in A^*, i.e., the location remains constant for a range of A^* and then jumps to another value for the next range of A^*.

Forced vibration data are compared with free vibration data for $Re = 100$. Morse and Williamson[16,17] carried out a similar analysis at high Re. An energy map is obtained using the results of forced vibration that gives the value of energy transfer per cycle of cylinder oscillation from the flow to the cylinder for a given A^* and f_y/f_{v_o}. The free vibration response for zero structural damping lies on the zero energy contour of the map. The lock-in regime obtained via free and forced vibration is found to be in excellent agreement.

ACKNOWLEDGMENTS

The authors acknowledge the use of computational resources at High Performance Computing facility, Computer Center, Indian Institute of Technology Kanpur that has been set up with the assistance from the Department of Science and Technology (DST), India.

APPENDIX: EFFECT OF MESH AND TIME STEP SIZE

We refer to the mesh that has been used for computations in this work as $M1$. To study the effect of grid refinement, a few cases are also computed using a finer mesh. The finer mesh, denoted by $M2$, consists of approximately twice the number of elements in $M1$. The size of the domain is identical for the two meshes. $(f^*, A^*) = (1.2, 0.75)$ has been selected to demonstrate the effect of mesh refinement on numerical results. This case corresponds to the largest frequency and amplitude of cylinder oscillation in the present work. Table II summarizes the results from computations carried out on the two

TABLE II. Flow past an oscillating cylinder with $(f^*, A^*) = (1.2, 0.75)$: summary of aerodynamic coefficients for two different finite element meshes.

Mesh	Nodes	Elements	$C_{L_{max}}$	$C_{L_{rms}}$	$C_{D_{avg}}$	$C_{D_{rms}}$
M1	11 256	10 988	0.8744	0.6471	2.4035	0.7501
M2	20 404	20 046	0.8855	0.6609	2.4046	0.7624

TABLE III. Flow past an oscillating cylinder with $(f^*, A^*) = (1.2, 0.75)$: summary of aerodynamic coefficients for computations carried out with $M1$ using two time step sizes.

Δ t	$C_{L_{max}}$	$C_{L_{rms}}$	$C_{D_{avg}}$	$C_{D_{rms}}$
0.1	0.8744	0.6471	2.4035	0.7501
0.01	0.8662	0.6545	2.4719	0.7398

meshes. The two sets of results are in excellent agreement. The differences in the average and fluctuating component of fluid forces are less than 2%. In view of the relative insensitivity of the aerodynamic quantities to mesh refinement beyond $M1$, we use $M1$ for all the computations.

Next, we investigate the effect of time step size. The test case is the same as that used for mesh convergence study, i.e., $(f^*, A^*) = (1.2, 0.75)$. Mesh M1 is used with two different time step sizes: $\Delta t = 0.1$ and $\Delta t = 0.01$. The results are summarized in Table III. It is noted that the two sets of results are in very good agreement. Among all quantities, the maximum difference is in $C_{D_{rms}}$. It is approximately 3%. The difference in the other quantities is less than 1%. Therefore, $\Delta t = 0.1$ is utilized for all the computations.

[1] R. D. Blevins, *Flow-Induced Vibration* (Van Nostrand Reinhold Co., Inc., New York, NY, USA, 1990).
[2] M. P. Païdoussis, S. J. Price, and E. De Langre, *Fluid-Structure Interactions: Cross-Flow-Induced Instabilities* (Cambridge University Press, 2010).
[3] T. Nakamura, S. Kaneko, F. Inada, M. Kato, K. Ishihara, T. Nishihara, N. W. Mureithi, and M. A. Langthjem, *Flow-Induced Vibrations: Classifications and Lessons from Practical Experiences* (Butterworth-Heinemann, 2013).
[4] R. E. D. Bishop and A. Y. Hassan, "The lift and drag forces on a circular cylinder oscillating in a flowing fluid," Proc. R. Soc. A **277**, 51–75 (1964).
[5] G. H. Koopmann, "The vortex wakes of vibrating cylinders at low Reynolds numbers," J. Fluid Mech. **28**, 501–512 (1967).
[6] C. H. K. Williamson, "Oblique and parallel modes of vortex shedding in the wake of a circular cylinder at low Reynolds numbers," J. Fluid Mech. **206**, 579–627 (1989).
[7] S. Mittal and G. Sidharth, "Steady forces on a cylinder with oblique vortex shedding," J. Fluid. Struct. **44**, 310–315 (2014).
[8] Navrose and S. Mittal, "Vibrations of a cylinder in a uniform flow in the presence of a no-slip side-wall," J. Fluid. Struct. **57**, 185–195 (2015).
[9] G. E. Karniadakis and G. S. Triantafyllou, "Frequency selection and asymptotic states in laminar wakes," J. Fluid Mech. **199**, 441–469 (1989).
[10] J. R. Meneghini and P. W. Bearman, "Numerical simulation of high amplitude oscillatory flow about a circular cylinder," J. Fluid. Struct. **9**, 435–455 (1995).
[11] M. R. H. Nobari and H. Naderan, "A numerical study of flow past a cylinder with cross flow and inline oscillation," Comput. Fluids **35**, 393–415 (2006).
[12] P. Anagnostopoulos, "Numerical study of the flow past a cylinder excited transversely to the incident stream. Part 1: Lock-in zone, hydrodynamic forces and wake geometry," J. Fluid. Struct. **14**, 819–851 (2000).
[13] T. Staubli, "Calculation of the vibration of an elastically mounted cylinder using experimental data from forced oscillation," J. Fluids Eng. **105**, 225–229 (1983).
[14] C. Feng, "The measurement of vortex induced effects in flow past stationary and oscillating circular and D-section cylinders," Ph.D. thesis, University of British Columbia, 1968.
[15] C. H. K. Williamson and A. Roshko, "Vortex formation in the wake of an oscillating cylinder," J. Fluid. Struct. **2**, 355–381 (1988).
[16] T. L. Morse and C. H. K. Williamson, "Employing controlled vibrations to predict fluid forces on a cylinder undergoing vortex-induced vibration," J. Fluid. Struct. **22**, 877–884 (2006).
[17] T. L. Morse and C. H. K. Williamson, "Fluid forcing, wake modes, and transitions for a cylinder undergoing controlled oscillations," J. Fluid. Struct. **25**, 697–712 (2009), Bluff Body Wakes and Vortex-Induced Vibrations (BBVIV-5).
[18] J. S. Leontini, B. E. Stewart, M. C. Thompson, and K. Hourigan, "Wake state and energy transitions of an oscillating cylinder at low Reynolds number," Phys. Fluids **18**, 067101 (2006).
[19] T. K. Prasanth and S. Mittal, "Vortex-induced vibrations of a circular cylinder at low Reynolds numbers," J. Fluid Mech. **594**, 463–491 (2008).
[20] T. E. Tezduyar, M. Behr, and J. Liou, "A new strategy for finite element computations involving moving boundaries and interfaces—The deforming-spatial-domain/space-time procedure: I. The concept and the preliminary numerical tests," Comput. Methods Appl. Mech. Eng. **94**, 339–351 (1992).
[21] T. E. Tezduyar, M. Behr, S. Mittal, and J. Liou, "A new strategy for finite element computations involving moving boundaries and interfaces—The deforming-spatial-domain/space-time procedure: II. Computation of free-surface flows, two-liquid flows, and flows with drifting cylinders," Comput. Methods Appl. Mech. Eng. **94**, 353–371 (1992).
[22] T. E. Tezduyar, S. Mittal, S. E. Ray, and R. Shih, "Incompressible flow computations with stabilized bilinear and linear equal-order-interpolation velocity-pressure elements," Comput. Methods Appl. Mech. Eng. **95**, 221–242 (1992).
[23] S. Mittal, "Stabilized space-time finite element formulations for unsteady incompressible flows involving fluid-body interactions," Ph.D. thesis, University of Minnesota, Minneapolis, 1992.

[24] S. Mittal and T. E. Tezduyar, "A finite element study of incompressible flows past oscillating cylinders and aerofoils," Int. J. Numer. Methods Fluids **15**, 1073–1118 (1992).
[25] Navrose and S. Mittal, "Free vibrations of a cylinder: 3-D computations at Re = 1000," J. Fluid. Struct. **41**, 109–118 (2013).
[26] M. Furquan, Navrose, and S. Mittal, "A fast mesh moving scheme for flow-induced vibrations of rigid bodies," Comput. Fluids **141**, 116–123 (2016).
[27] R. Govardhan and C. Williamson, "Defining the modified griffin plotin vortex-induced vibration: Revealing the effect of Reynolds number using controlled damping," J. Fluid Mech. **561**, 147–180 (2006).
[28] Navrose, V. Yogeswaran, S. Sen, and S. Mittal, "Free vibrations of an elliptic cylinder at low Reynolds numbers," J. Fluid. Struct. **51**, 55–67 (2014).
[29] Navrose and S. Mittal, "A new branch, IB(II), in free vibration of a cylinder at low Re," J. Fluid. Struct. (to be published).
[30] S. P. Singh and S. Mittal, "Vortex-induced oscillations at low Reynolds numbers: Hysteresis and vortex-shedding modes," J. Fluid. Struct. **20**, 1085–1104 (2005).